

# A model of troponin-I in complex with troponin-C using hybrid experimental data: The inhibitory region is a $\beta$ -hairpin

CHANG-SHUNG TUNG,<sup>1</sup> MICHAEL E. WALL,<sup>2</sup> STEPHEN C. GALLAGHER,<sup>2</sup>  
AND JILL TREWHELLA<sup>2</sup>

<sup>1</sup>Theoretical Division, Los Alamos National Laboratory, Los Alamos, New Mexico 87545

<sup>2</sup>Bioscience Division, Los Alamos National Laboratory, Los Alamos, New Mexico 87545

(RECEIVED November 3, 1999; FINAL REVISION May 8, 2000; ACCEPTED May 11, 2000)

## Abstract

We present a model for the skeletal muscle troponin-C (TnC)/troponin-I (TnI) interaction, a critical molecular switch that is responsible for calcium-dependent regulation of the contractile mechanism. Despite concerted efforts by multiple groups for more than a decade, attempts to crystallize troponin-C in complex with troponin-I, or in the ternary troponin complex, have not yet delivered a high-resolution structure. Many groups have pursued different experimental strategies, such as X-ray crystallography, NMR, small-angle scattering, chemical cross-linking, and fluorescent resonance energy transfer (FRET) to gain insights into the nature of the TnC/TnI interaction. We have integrated the results of these experiments to develop a model of the TnC/TnI interaction, using an atomic model of TnC as a scaffold. The TnI sequence was fit to each of two alternate neutron scattering envelopes: one that winds about TnC in a left-handed sense (Model L), and another that winds about TnC in a right-handed sense (Model R). Information from crystallography and NMR experiments was used to define segments of the models. Tests show that both models are consistent with available cross-linking and FRET data. The inhibitory region TnI(95–114) is modeled as a flexible  $\beta$ -hairpin, and in both models it is localized to the same region on the central helix of TnC. The sequence of the inhibitory region is similar to that of a  $\beta$ -hairpin region of the actin-binding protein profilin. This similarity supports our model and suggests the possibility of using an available profilin/actin crystal structure to model the TnI/actin interaction. We propose that the  $\beta$ -hairpin is an important structural motif that communicates the  $\text{Ca}^{2+}$ -activated troponin regulatory signal to actin.

**Keywords:** actin-binding protein; calcium-binding protein; cross-linking; fast skeletal muscle contraction; FRET; profilin; small-angle neutron scattering; troponin; regulatory complex

The troponin complex sits on the thin filaments of vertebrate skeletal muscle and acts as a  $\text{Ca}^{2+}$ -sensitive switch that regulates the interactions between the thick and thin filaments, whose proposed sliding motions give rise to contraction. Troponin has three components: troponin C (TnC), which binds  $\text{Ca}^{2+}$  reversibly; troponin I (TnI), which inhibits actomyosin activity; and troponin T (TnT), which binds to tropomyosin and is proposed to be involved in the transmission of the regulatory signal along the thin filament (recent reviews in Farah & Reinach, 1995; Tobacman, 1996; Perry, 1999).  $\text{Ca}^{2+}$  binding to TnC initiates muscle contraction by causing TnI to release its inhibition of the interactions between the myosin headgroups of the thick filaments and the actin molecules of the thin filaments, thus switching on the acto-myosin activity that drives muscle contraction. Crystal structures are available for

both  $2\text{Ca}^{2+}/\text{TnC}$  (Satyshur et al., 1988, Protein Data Bank (PDB) accession 4TNC; Herzberg & James, 1988, PDB accession 5TNC) and  $4\text{Ca}^{2+}/\text{TnC}$  (Houdusse et al., 1997, PDB accessions 1TN4 and 2TN4; Soman et al., 1999, PDB accession 1TCF). In the crystal form, TnC has a dumbbell shape with two globular domains separated by an extended, solvent-exposed helix of 7–8 turns that is flexible in solution (Heidorn & Trewhella, 1988; Blechner et al., 1992; Slupsky & Sykes, 1995). Each globular domain consists of a pair of  $\text{Ca}^{2+}$ -binding EF-hand motifs (Kretsinger, 1976). In muscle, the C-terminal domain is occupied by  $\text{Ca}^{2+}$ , even in the absence of a  $\text{Ca}^{2+}$  signal. The N-terminal domain is alternately occupied by  $\text{Mg}^{2+}$  or  $\text{Ca}^{2+}$  as the  $\text{Ca}^{2+}$  level fluctuates in the cell (Potter & Gergely, 1975). The effect of 2 mol equivalent  $\text{Ca}^{2+}$  binding to either lobe is to open the cup-shaped domain structure, exposing hydrophobic residues on the inner surface (Herzberg et al., 1986; Gagné et al., 1995; Strynadka et al., 1997). This conformational change in the N-terminal lobe is believed to be key to regulating the interactions of TnC and TnI.

Reprint requests to: Michael Wall, Bioscience Division, B-1, MS G758, Los Alamos National Laboratory, Los Alamos, New Mexico 87545; e-mail: mewall@lanl.gov.

To date, there is no crystal structure available either for TnC in complex with intact TnI, or for the ternary TnC/TnI/TnT troponin complex. The lack of high-resolution data for the regulatory assembly has impeded understanding of the molecular basis for its switching function. Many groups have pursued different experimental strategies to gain insights into the nature of the TnC/TnI interaction. Binding and activity assays, using peptides and mutant proteins, have defined a number of important regions in TnI that interact with TnC (Chandra et al., 1994; Pearlstone & Smillie, 1995; Pearlstone et al., 1997; Tripet et al., 1997; Kobayashi et al., 1999; Szczesna et al., 1999). Cross-linking (Leszyk et al., 1987, 1988, 1990; Kobayashi et al., 1991, 1994, 1996; Ngai et al., 1994; Jha et al., 1996; Luo et al., 1999) and FRET data (Wang & Cheung, 1984; Tao et al., 1989; Luo et al., 1997, 1998) have provided distance information for the interactions. Neutron scattering contrast variation studies have provided shape and size information on TnC and TnI in the binary TnC/TnI complex (Olah et al., 1994; Olah & Trehwella, 1994) and in the ternary TnC/TnI/TnT troponin complex (Stone et al., 1998). NMR studies of TnC with various TnI peptides have yielded detailed information on the structure of N-TnC when bound to TnI (McKay et al., 1998, PDB accession 1BLQ) and have yielded some structural information on the peptides (Campbell & Sykes, 1991; Hernández et al., 1999) and TnC/TnI interactions (McKay et al., 1997, 1998, 1999). Recently, the NMR structure of the cardiac TnI peptide fragment TnI(147–163) in complex with the N-domain of cardiac TnC has been solved (Li et al., 1999; PDB accession 1MXL), and the crystal structure of TnC in complex with the TnI N-terminal peptide fragment TnI(1–47) has been solved (Vassilyev et al., 1998; PDB accession 1A2X).

This paper describes two alternative models of the TnC/TnI complex that are consistent with currently available experimental data on the TnC/TnI interaction. In both models, TnC is extended and is the same as the modified crystal structure in our previous neutron scattering model (Olah & Trehwella, 1994). The overall fold of TnI was derived from two alternate neutron scattering envelopes, both consistent with the scattering data, and related to one another by an inversion through the center of mass. In Model L, TnI winds about the central helix of TnC in a left-handed sense, while in Model R the sense is right-handed. All-atom models for TnI were fit into these folds, and fragments were positioned using information from published crystallography and NMR studies. Based on NMR and circular dichroism (CD) data obtained in our laboratory (Hernández et al., 1999), the inhibitory region was modeled as a flexible  $\beta$ -hairpin; the hairpin is in the same position in both models of the complex. This structural motif, its location with respect to TnC, and its sequence similarity with profilin suggest a basis for the  $\text{Ca}^{2+}$ -sensitive switching mechanism of the complex. Model stereochemistry was improved by simple energy minimization and by molecular dynamics using an energy function derived from a database of interatomic distance probabilities (Wall et al., 1999). The resultant models provide a framework for discussion and for developing further experiments for testing and refinement. Such a framework is critical to furthering our understanding of the molecular basis for troponin's switching function in the contractile cycle.

## Results

The TnC/TnI models are depicted in Figure 1, Model L at the left, and Model R at the right. They have been deposited at the Protein Data Bank (Berman et al., 2000; accessible at <http://www.rcsb.org>)

under accession code 1EW7. The TnC and TnI polypeptide chains are aligned in an antiparallel sense, with the N-terminal domain of TnI interacting with the C-terminal domain of TnC and vice versa. This arrangement agrees with that implied by the deletion mutation study on skeletal muscle TnI (Farah et al., 1994) and the NMR study of a cardiac TnC/TnI complex (Krudy et al., 1994). The overall topology of TnI and TnC in the models also explains how two relatively small proteins of comparable molecular weight can interact with each other extensively over the length of their respective sequences, as is indicated by the accumulated cross-linking and fluorescence data. Binding affinity studies involving TnC double alanine mutants (Kobayashi et al., 1999) indicate that TnC residues 85 and 86 influence the interaction of TnC with TnI residues 117–124, which is also consistent with the relative disposition of TnC and TnI in our modeling.

### Model for TnC in the complex

At the time of the neutron study of the  $4\text{Ca}^{2+}$ /TnC/TnI binary complex (Olah et al., 1994), only the crystal structure of  $2\text{Ca}^{2+}$ /TnC had been solved (Herzberg & James, 1988; Satyshur et al., 1988). A modeling study showed that the best fit to the neutron data could be obtained by preserving the extended central helix of the  $2\text{Ca}^{2+}$ /TnC crystal structure, and opening the N-terminal  $\text{Ca}^{2+}$ -binding domain (Olah & Trehwella, 1994). This opening mimicked the open configuration observed for the  $\text{Ca}^{2+}$ -saturated C-domain and resulted in the exposure of the N-domain hydrophobic cleft, as proposed by Herzberg et al. (1986). Recent crystal structures of  $4\text{Ca}^{2+}$ /TnC (Houdusse et al., 1997; Soman et al., 1999) show an extended central helix and an open C-domain that are very similar to those in the both the  $2\text{Ca}^{2+}$ /TnC structure and the neutron scattering model. The N-domain in the  $4\text{Ca}^{2+}$ /TnC structure is more open than that in the  $2\text{Ca}^{2+}$ /TnC structure, but it is more closed than is required to fit the neutron scattering data, possibly as a result of crystal packing or the binding of TnI. The degree of opening in the hydrophobic cleft reported by Sykes et al. in their NMR studies of  $2\text{Ca}^{2+}$ /N-TnC (Gagné et al., 1995) and  $2\text{Ca}^{2+}$ /N-TnC/TnI(96–148) (McKay et al., 1998; PDB accession 1BLQ) agrees well with that described in our neutron scattering model, and is significantly more than that observed in the  $4\text{Ca}^{2+}$ /TnC crystal structures (Houdusse et al., 1997; Soman et al., 1999). Use of the  $4\text{Ca}^{2+}$ /TnC crystal structures in our model of the complex therefore would require an opening of N-TnC, similar to the procedure performed in generating the neutron scattering model. Due to (1) the need to modify the available  $4\text{Ca}^{2+}$ /TnC crystal structures to enable them to be used; (2) the present agreement between the neutron scattering model of TnC in complex with TnI and the NMR studies; and (3) the fact that the neutron scattering model for the binary complex is based on data from intact proteins, we used the TnC coordinates from the neutron scattering model (Olah & Trehwella, 1994) as the scaffold for building the model of TnI (see Fig. 2).

### Models for TnI in the complex

The neutron-derived model for the  $4\text{Ca}^{2+}$ /TnC/TnI complex shows TnI as a supercoiled structure (Fig. 2), with two end-cap regions (not shown) that have minimal contact with TnC, and that most likely correspond to loosely structured regions of the protein (Olah & Trehwella, 1994). The neutron data in fact allow for two possible configurations for TnI in its interaction with TnC: in Model

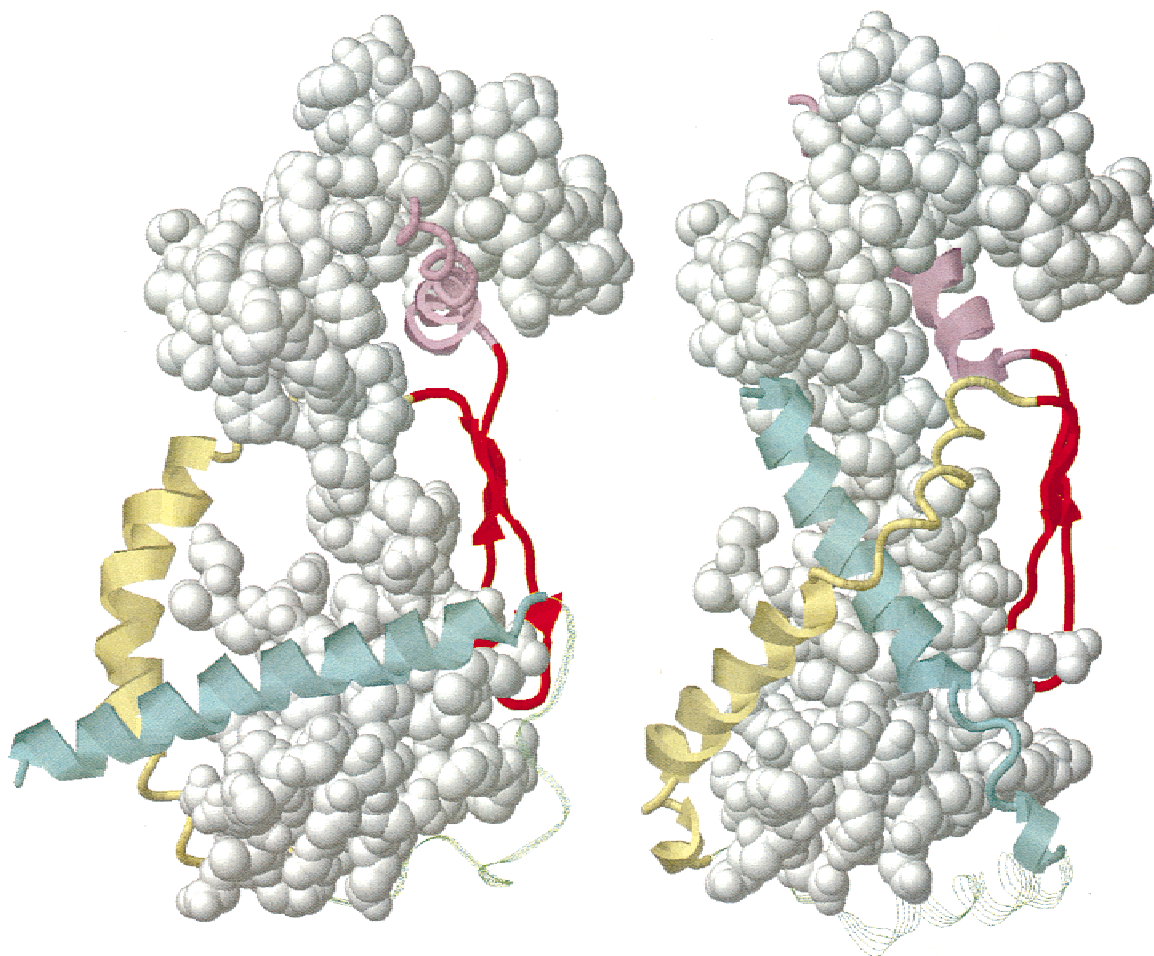


**Fig. 1.** Ribbon models of TnI in complex with TnC. TnC (white) is shown as Van der Waals spheres with the N-domain at the top. TnI is shown in five segments: Segment I (cyan), TnI(3–33); Segment II (green strands), TnI(34–53); Segment III (yellow), TnI(54–94); Segment IV inhibitory region (red), TnI(95–114); Segment V (pink), TnI(115–134). In the model at the left (Model L), segments III and V together coil around TnC in a left-handed sense. In the model at the right (Model R), segments III and V coil around TnC in a right-handed sense.

L, the supercoiled structure winds about TnC in a left-handed sense; in Model R, the sense is right-handed. The two TnI models are related by an inversion through the origin, and both are allowable because (1) the shape of TnC is approximately conserved upon inversion, and (2) neutron scattering data are identical for two structures that are related by an inversion through the origin. Figure 2 shows the R form that was originally presented by Olah and Trewthella (1994). While that study considered the alternative handedness, the R form was selected because it appeared to be favored by the limited cross-linking data available at the time. Our more extensive analysis using presently available cross-linking data leads us to conclude that both models are equally likely. In both models, the supercoil, which has the dimensions of a single  $\alpha$ -helix, passes near the C-terminal hydrophobic cleft of TnC, winds around the extended TnC structure, and passes through the N-terminal hydrophobic cleft.

The five contiguous segments of TnI in our models, segments I through V, are color-coded in Figure 1 and correspond to residues 3–33, 34–53, 54–94, 95–114, and 115–134, respectively (Fig. 3). In the crystal structure of TnC/TnI(1–47) (Vassilyev et al., 1998),

there is no electron density visible for TnI residues 1–2 and 34–47. Residues 1–2 are therefore not included in the structural model, and we define segment I such that it ends at residue 33. Segment VI (residues 135–181) is also not included in the model, as there are no available structural constraints, and NMR data indicate that TnI residues C-terminal to residue 136 are unstructured when in complex with the N-terminal fragment of TnC (McKay et al., 1999).

#### *TnI Segment I*

In both models segment I (residues 3–33) is an  $\alpha$ -helix that packs into the hydrophobic cleft of the C-domain of TnC. The  $\alpha$ -helix and its interaction with TnC is based on the crystal structure of TnI(1–47) in complex with TnC (Vassilyev et al., 1998; PDB accession number 1A2X). In Model L, the detailed interaction between segment I and TnC is preserved, while in Model R the positioning of segment I was reoriented to avoid clashes with segment III of TnI. In the crystal structure, TnC is partially collapsed, bringing TnI(1–47) into contact with the N-domain of TnC. As TnC is extended in our models, TnI(1–47) does not make



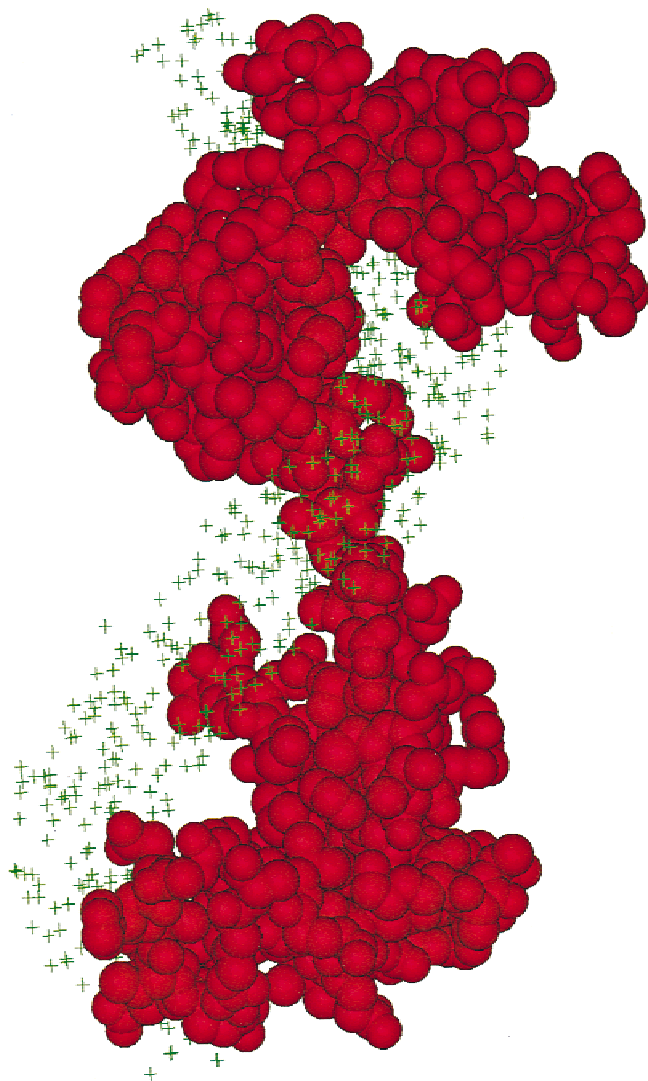


**Fig. 2.** Neutron scattering model of  $4\text{Ca}^{2+}/\text{TnC}/\text{TnI}$ . This model, taken from Olah and Trehwella (1994), was used to build the structure of TnI in Model R. TnC (red) is shown as Van der Waals spheres, and the supercoiled region of TnI is shown as a volume filled with green crosses. The dimensions of the TnI spiral are consistent with the structure being a single supercoiled  $\alpha$ -helix. TnI segments V and III were fit into the spiral.

contact with the N-domain of TnC in Model L. In Model R segment I is rotated by  $\sim 90^\circ$  with respect to the crystal structure and aligns with the central helix. A consequence of this rotation is that TnI(1–47) makes contact with the N-terminal domain of TnC in Model R. An analysis of close contacts between TnI(1–47) and TnC in the crystal structure shows that, in model R,  $\text{C}\alpha$  atom pairs corresponding to crystal-structure contacts between TnC and TnI (see Materials and methods) stayed within  $9.5 \text{ \AA}$  of each other for all TnI residues with a few exceptions. In both models, residues 4, 7, and 11 do not make contact with the N-domain of TnC due to the extended conformation of TnC. In addition, contacts involving residues 14 and 19 are lost in Model R due to the rotation of segment I relative to its orientation in the crystal structure.

#### *TnI segment II*

In both models, the structures shown for segment II (residues 34–53) are selected from many alternatives for joining the ends of

segments I and III. The neutron scattering data show only diffuse features in the appropriate region of the molecule (Olah & Trehwella, 1994), and there was no electron density observed for residues 34–47 in the crystal structure of TnC/TnI(1–47) (Vasyliev et al., 1998). It is possible that segment II acts as a flexible tether between segment I, which binds to TnC, and segment III, which binds to TnT (Pearlstone & Smillie, 1985; Stefancsik et al., 1998; Luo et al., 2000), co-localizing TnC and TnT even under conditions of low cellular  $\text{Ca}^{2+}$ .

#### *TnI segment III*

We modeled segment III in the binary complex as an  $\alpha$ -helix that fits into the supercoiled TnI envelope derived from the neutron scattering data. This supercoiled structure is consistent with studies suggesting that TnI(53–106), which contains segment III (residues 54–94), binds to TnT(205–255) in a coiled-coil interaction (Pearlstone & Smillie, 1985; Stefancsik et al., 1998), and that TnI<sup>48</sup>, TnI<sup>64</sup>, and TnI<sup>89</sup> come close enough to TnT to be cross-linked using BP-Mal (Luo et al., 2000). It is also consistent with the  $\alpha$ -helical secondary-structure prediction for this segment (Fig. 3). The helix in model R follows the neutron scattering model for TnI that winds about TnC in a right-handed sense (Olah et al., 1994) (Fig. 2) and packs tightly against the central helix of TnC. The helix in model L follows an inverted neutron scattering model that winds about TnC in a left-handed sense and forms a handle-like feature that travels from the N-domain to the C-domain of TnC, leaving a gap between itself and the TnC central helix.

#### *TnI segment IV, the inhibitory region*

Segment IV (residues 95–114) of TnI corresponds to the so-called inhibitory sequence of TnI. This fragment alone can fully inhibit acto-myosin ATPase activity (Syska et al., 1976) and has been proposed to bind alternately to actin and TnC during the contractile cycle (Van Eyk et al., 1993). We propose that segment IV adopts a  $\beta$ -hairpin structure, aligned with the central helix of TnC in the  $4\text{Ca}^{2+}$ -bound state. The  $\beta$ -hairpin connects with segments III and V at the stem. In both models, residues 104 and 105 are in the hairpin loop near the C-domain of TnC, and residues 96–103 and 106–113 are in the stem that points toward the N-domain of TnC. Such a structure is suggested by recent NMR experiments (Hernández et al., 1999) indicating that the inhibitory peptide is extended when bound to TnC, with a kink at Gly104. Residues 95 and 103 connect the hairpin to segments III and V. Although the available constraints cannot be used to define the precise conformation of segment IV, our proposed placement of the  $\beta$ -hairpin with respect to TnC satisfies the cross-linking and fluorescence data that implicate this relatively short inhibitory sequence as interacting with both N- and C-terminal lobes of TnC (see below).

Supporting evidence for our  $\beta$ -hairpin conformation for segment IV comes from a sequence comparison between TnI and profilin, a protein which is known to play a role in actin filament assembly in the cytoskeleton (Carlsson et al., 1977). We found that TnI residues TnI(101–132) align with residues 86–118 of profilin, with a single-residue gap inserted at TnI 109 (Fig. 6; see Materials and methods). This alignment places TnI inhibitory region residues 96–117 in register with profilin residues 81–103. Using the crystal structure coordinates of the profilin/actin complex (Schutt et al., 1995; PDB accession 2BTF), we have identified some striking similarities between TnI and profilin. First, comparing data from a chemical cross-linking experiment involving TnI and actin (Tao et al., 1990) and the profilin/actin crystal structure, it appears that

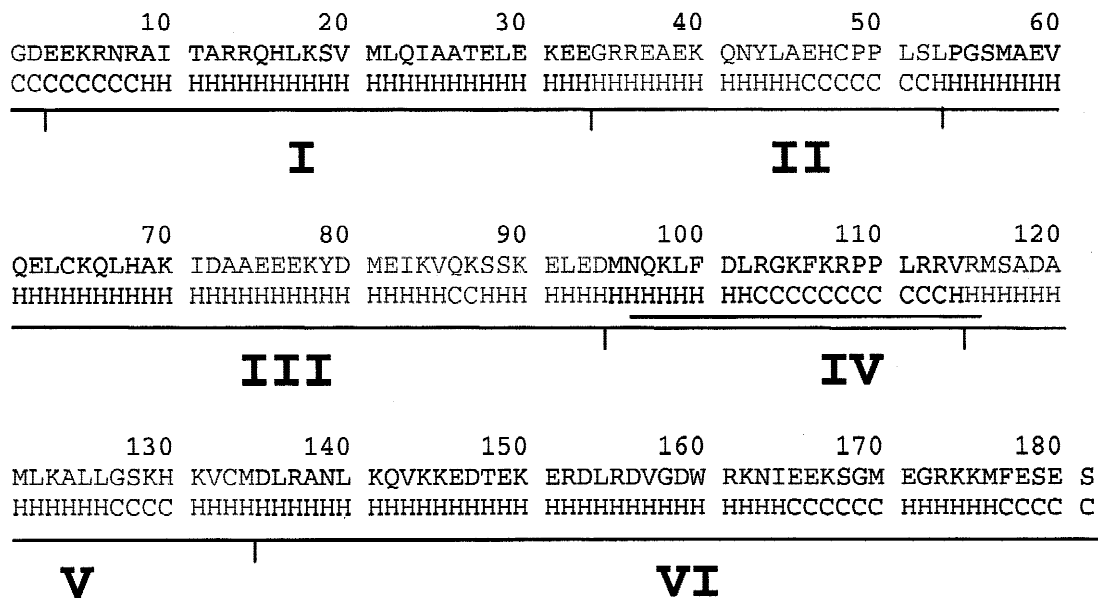


**Fig. 3.** Secondary structure prediction for each segment of TnI. Predictions for helix (H) and coil (C) are indicated beneath the corresponding amino acid in the sequence. Segments I–VI are labeled, and the inhibitory region is underlined. The rabbit fast skeletal muscle TnI sequence is from Wilkinson and Grand (1978) (Swiss-Prot accession P02643). The prediction is a consensus derived using a number of different methods: SOPMA (Georjun & Deleage, 1994, 1995), Gibrat (Georjun & Deleage, 1994, 1995), Levin (Levin et al., 1986), DPM (Deleage & Roux, 1987), and PHD (Rost & Sander, 1994).

both profilin and TnI bind in the same region of actin. The experiment shows that in the absence of  $\text{Ca}^{2+}$ , TnI Cys133 comes within 9 Å of actin Cys374 (close enough to be cross-linked using BP-Mal). Actin Cys374 participates in binding to profilin, and, using our local sequence alignment (Fig. 6), TnI Cys133 corresponds to profilin His119, the C $\gamma$  of which is just 8.7 Å from the S $\gamma$  of actin Cys374 (see Fig. 7). Also, profilin residues 81–103 (corresponding to residues 96–117 of TnI) are at the profilin/actin interface and form a  $\beta$ -hairpin with a right-handed twist (see Fig. 7), similar to the structure that we have proposed for TnI segment IV (Fig. 1). In addition to providing evidence for a  $\beta$ -hairpin conformation of segment IV, these findings suggest that available profilin crystal structures both with (Schutt et al., 1995; PDB accession 2BTF) and without actin (see, e.g., Nodelman et al., 1999; PDB accession 1D1J) may be useful for understanding the interactions between TnI and actin.

#### TnI segment V

In both models segment V (115–134) is an  $\alpha$ -helix that is cradled by the hydrophobic cleft of the N-domain of TnC and is an extension of the path of the supercoiled  $\alpha$ -helix of segment III. Both models conform to the neutron scattering envelope defined by the L and R models. In Model L, the helix leaves the  $\beta$ -hairpin and comes to the front of the N-domain of TnC (Fig. 1), similar to the placement found in NMR studies on both skeletal N-TnC/TnI(115–131) (Spyracopoulos et al., 2000) and cardiac N-TnC/TnI(147–163) (Li et al., 1999) (cardiac TnI(147–163) corresponds to skeletal TnI(115–131)). In Model R, the helix leaves the  $\beta$ -hairpin and goes to the back of the N-domain of TnC. The placement of this segment in model R is different from that found in the NMR studies of peptide fragments.

#### Refined model of TnI in complex with TnC

Models R and L both were refined using energy minimization and molecular dynamics to obtain improved stereochemistry (see Materials and methods). Evaluation using the program PROCHECK (Lasowski et al., 1993) shows that each model has acceptable geometry with all residues in allowed regions of the Ramachandran plot. Model R has 79% of residues in most favored regions, 17% in additional allowed regions, and 4% in generously allowed regions of the Ramachandran plot; Model L has 85% in most favored regions, 12% in additional allowed regions, and 3% in generously allowed regions.

#### Evaluation of the model against additional experimental constraints

Results of tests using cross-linking and FRET data are summarized in Tables 1 and 2, respectively. Figure 4 highlights residues in each model that are the best candidates for observed cross-links, and Figure 5 shows the positions of FRET donor and acceptor labels on each model. Both models are consistent with available cross-linking and FRET data. Distances were calculated between all atom pairs in each model that were identified as likely candidates for cross-linking based on published data (Table 1; see Materials and methods).

Five of the six cross-links between TnC and intact TnI have at least one corresponding interatomic distance in each model that would accommodate the cross-linking requirement (see Materials and methods for criteria). In addition, the model could be reasonably modified to allow a cross-link between TnC158 and TnI21. As TnC158 is the penultimate residue in the sequence, many alternate conformations of the C-terminal tail of TnC would allow TnC158 to come within cross-linking distance of TnI21, in agree-

**Table 1.** Distances between atoms that are candidates for cross-linking<sup>a</sup>

TnC	TnI segment <sup>b</sup>	TnI		$D_{\text{model}}^c$		$D_{\text{Ca}}^c$		$D_{\text{xl}}^c$	Source <sup>d</sup>
		R	L	R	L	R	L		
Ala21C $\beta$	96–134	Lys129C $\epsilon$	Val132C $\beta$	15.0	4.9	17.8	6.9	9	Lz1998
Gln48C $\gamma$	121	Met121C $\gamma$	Met121C $\gamma$	12.3	10.9	14.2	10.8	10	L1999
Ala57C $\beta$	113–121	Arg113C $\delta$	Arg115C $\delta$	10.1	6.3	14.9	7.6	9	K1991
Gln82C $\gamma$	121	Met121C $\gamma$	Met121C $\gamma$	3.8	6.2	6.6	11.0	10	L1999
Gly89C $\alpha$	108–113	Leu111C $\gamma$	Arg112C $\delta$	9.0	5.4	11.5	8.8	9	K1994
Cys98S $\gamma$	103–111	Arg103C $\delta$	Lys107C $\epsilon$	10.6	11.0	8.9	14.0	9	Lz1987/8
Val158C $\gamma_1$	21	Met21C $\gamma$	Met21C $\gamma$	19.9	16.9	20.7	16.9	9	Lz1998
Ala57C $\beta$	f98–114	Arg113C $\delta$	Val114C $\beta$	10.1	9.3	14.9	10.6	9	J1996
Glu60O $\epsilon_1$	f104–115	Arg113NH $_2$	Arg115NH $_2$	11.3	10.3	19.4	11.0	3	K1996
Glu61O $\epsilon_1$	f104–115	Arg113NH $_2$	Arg115NH $_2$	9.2	3.2	18.8	9.4	3	K1996
Cys98S $\gamma$	f98–114	Leu102C $\gamma$	Lys107C $\epsilon$	9.0	11.0	7.8	14.0	9	J1996
Asp133C $\gamma$	f98–114	Arg103C $\delta$	Lys107C $\epsilon$	26.3	25.0	25.3	27.6	9	J1996
Met155C $\gamma$	f104–115	Lys107C $\epsilon$	Lys107C $\epsilon$	17.8	13.1	21.5	18.1	9	N1994

<sup>a</sup>Criteria for including data in this table are described in Materials and methods. Residues for which cross-linking data are available from experiments on the binary complex are indicated in Figure 4.

<sup>b</sup>TnI segment is the segment on TnI to which the TnC cross-link is localized. Preceding “f” indicates that the experiment was performed using a peptide fragment consisting of the listed residues.

<sup>c</sup> $D_{\text{model}}$  = model distance between atoms designated in columns 1 and 2,  $D_{\text{xl}}$  = estimated distance based on cross-link used (EDC = 3 Å; BP-Mal = 9 Å; BP-IA = 10 Å),  $D_{\text{Ca}}$  = C $\alpha$  separation distance between residues designated in columns 1 and 2.

<sup>d</sup>Source of data: K1994, K1991, K1996 = Kobayashi et al. (1994, 1991, 1996); Lz1987/8, Lz1998 = Leszyk et al. (1987, 1988, 1998); J1996 = Jha et al. (1996); N1994 = Ngai et al. (1994); L1999 = Luo et al. (1999).

ment with the findings of Leszyk et al. (1998). Crystal structures of 4Ca<sup>2+</sup>/TnC (PDB accession numbers 1TCF, 1TN4, and 2TN4) support this possibility, as there is no observed electron density for the last few residues at the C-terminus of TnC. Model R does not

have any specific atom pairs that could correspond to observed cross-links between TnC21 and TnI(96–134) (Leszyk et al., 1998), but there are many C $\alpha$ -C $\alpha$  distances (<20 Å with long side chains) in Model R that could form cross-links if side chain orientations

**Table 2.** Interatomic distances obtained by FRET experiments with TnI labeled at Cys133<sup>a</sup>

FRET partner	Donor/acceptor <sup>b</sup>	$D_{\text{model}}^c$		$D_{\text{Ca}}^c$		$D_F^c$	$L_D^c$	$L_A^c$	Source <sup>d</sup>
		R	L	R	L				
TnC Ala5C $\beta$	IAEDANS/DDP-MAL	18.7	29.2	16.3	27.2	31	12	9	L1998
TnI Ser12O $\gamma$	IAEDANS/DDP-MAL	24.5	17.2	22.6	18.6	19	12	9	L1998
TnC Ala21C $\beta$	IAEDANS/DDP-MAL	18.7	8.8	18.8	8.7	29	12	9	L1998
TnC Met25S $\delta$	DNZ/IAE	18.8	10.7	17.6	11.9	23	3	12	W1984
TnC Thr41C $\gamma_2$	IAEDANS/DAB-MAL	21.4	21.5	22.5	21.2	37	12	9	L1998
TnC Asn49C $\gamma$	IAEDANS/DAB-MAL	27.9	23.1	27.4	22.4	39	12	9	L1998
TnC Gly89C $\alpha^e$	IAEDANS/DDP-MAL	31.8	29.1	31.0	30.7	29	12	9	L1998
TnC Cys98S $\gamma$	IAEDANS/DDP-MAL	44.3	36.3	45.1	37.9	30	12	9	L1998
TnC Cys98S $\gamma$	IAEDANS/DAB-MAL	44.3	36.3	45.1	37.9	40	12	9	T1989
TnC Asp133C $\gamma^e$	IAEDANS/DAB-MAL	57.7	50.7	56.9	52.8	43	12	9	L1998
TnI Cys48S $\gamma$	IAEDANS/DAB-MAL	65.9	58.4	67.0	58.6	43	12	9	L1997
TnI Cys48S $\gamma^f$	IAEDANS/DAB-MAL	65.9	58.4	67.0	58.6	67	12	9	L1997

<sup>a</sup>Unless otherwise indicated, experiments were performed using the binary TnC/TnI complex in the presence of Ca<sup>2+</sup>. Residues for which FRET data are available from experiments on the binary complex are indicated in Figure 5. All distances are in Å.

<sup>b</sup>DNZ = dansylaziridine; IAE = 5'-(iodoacetamido)eosin; IAEDANS = N-iodoacetyl-N'-(5-sulfo-1-naphthyl)ethylenediamine; DDP-Mal = N-(4-dimethylamino-3,5-dinitrophenyl)maleimide; DAB-Mal = 4-dimethylaminophenylazophenyl-4'-maleimide.

<sup>c</sup> $D_{\text{model}}$  = distance in model between TnI Cys133S $\gamma$  and the FRET partner atom;  $D_{\text{Ca}}$  = distance between C $\alpha$  positions in model;  $D_F$  = distance measured by FRET (the uncertainty is roughly 20–25% (Tao et al., 1989));  $L_D$  = approximate length of donor, as measured from the covalently attached atom on the protein to the fluorescent center;  $L_A$  = approximate length of acceptor, determined as for  $L_D$ .

<sup>d</sup>Source of data: W1984 = Wang & Cheung (1984); T1989 = Tao et al. (1989); L1997, L1998 = Luo et al. (1997, 1998).

<sup>e</sup>This experiment was performed using the ternary TnC/TnI/TnT complex in the presence of Ca<sup>2+</sup>.

<sup>f</sup>This experiment was performed using the TnC/TnI/TnT/Tm/actin synthetic filament in the presence of Mg<sup>2+</sup>.

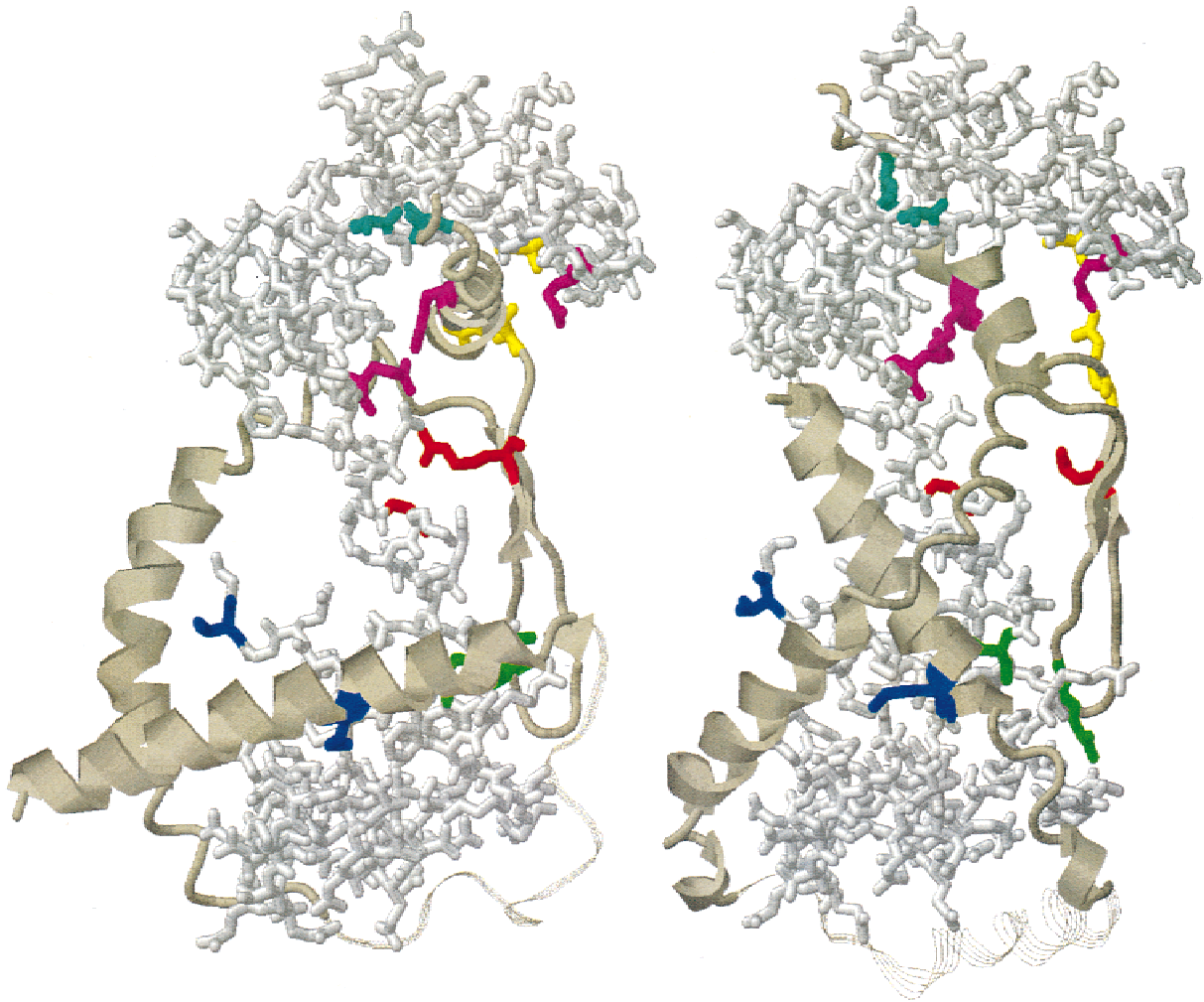


**Fig. 4.** Residues that can participate in observed cross-links. TnC is rendered as a wireframe, and key side chains on TnI are rendered as wireframes on a ribbon backbone. Residue pairs that are the best candidates for making cross-links are colored identically. The candidate TnI residues are listed in Table 1. The cross-linked partner residues on TnC are: TnC21 (cyan); TnC48 and TnC82 (magenta); TnC57 (yellow); TnC89 (red); TnC98 (green); TnC158 (blue). Three residues are colored magenta because TnC48 and TnC82 both form cross-links with TnI121.

were favorable. The model also has an Ala as opposed to the Cys at TnC21 used in the cross-linking experiments, forcing model distances to be measured from a  $C\beta$ , which is closer to the backbone than the  $S\gamma$  in the Cys where the BP-Mal is attached. Finally, multiple cross-linking sites were identified throughout TnI (96–134), indicating that Leszyk et al. (1998) observed structural variability in this region of the binary complex.

Of the six cross-links reported between TnC and TnI fragments, two have supporting interatomic distances in both models, and both of these cross-links are also reported in experiments with intact TnI. Model L has a supporting interatomic distance for one of the remaining four cross-links, and model R has no supporting interatomic distances for these cross-links. That some of the cross-linking distances involving peptide fragments are not found in our models could be attributed to the fact that the inhibitory peptide binds with low affinity ( $\sim 10^{-6} K_D$ ) and has been shown to bind at multiple sites on TnI (Pearlstone & Smillie, 1995; Jha et al., 1996; Kobayashi et al., 1996). Another reported cross-link, between the

C-terminus of TnI (residues 132–141) and residue 12 of TnC (Kobayashi et al., 1994), cannot be used for validation, as our models end at TnI134. NMR data of McKay et al. (1999), however, indicate TnI residues immediately C-terminal to 136 are unstructured, which would allow either model to accommodate this cross-link.

The models are consistent with all of the 11 FRET distances measured between a label at TnI Cys133 and labels at residues in TnC and TnI (Table 2). Three of the FRET distances listed, involving TnC residues 21, 89, and 133, were only available from an experiment with the  $4Ca^{2+}$ /TnC/TnI/TnT ternary complex (Luo et al., 1998). In one experiment by Luo et al. (1997), FRET was measured between residues TnI48 and TnI133 in binary and ternary complexes, and in reconstituted thin filaments, with different divalent ions. For the  $Ca^{2+}$ -loaded binary TnI/TnC complex, the FRET distance was determined to be 43 Å, which is consistent with model L and agrees with Model R only just within uncertainties. For the  $Mg^{2+}$ -loaded TnI/TnC/TnT/Tm/actin complex, however, the FRET distance was measured to be 67 Å, which is closer



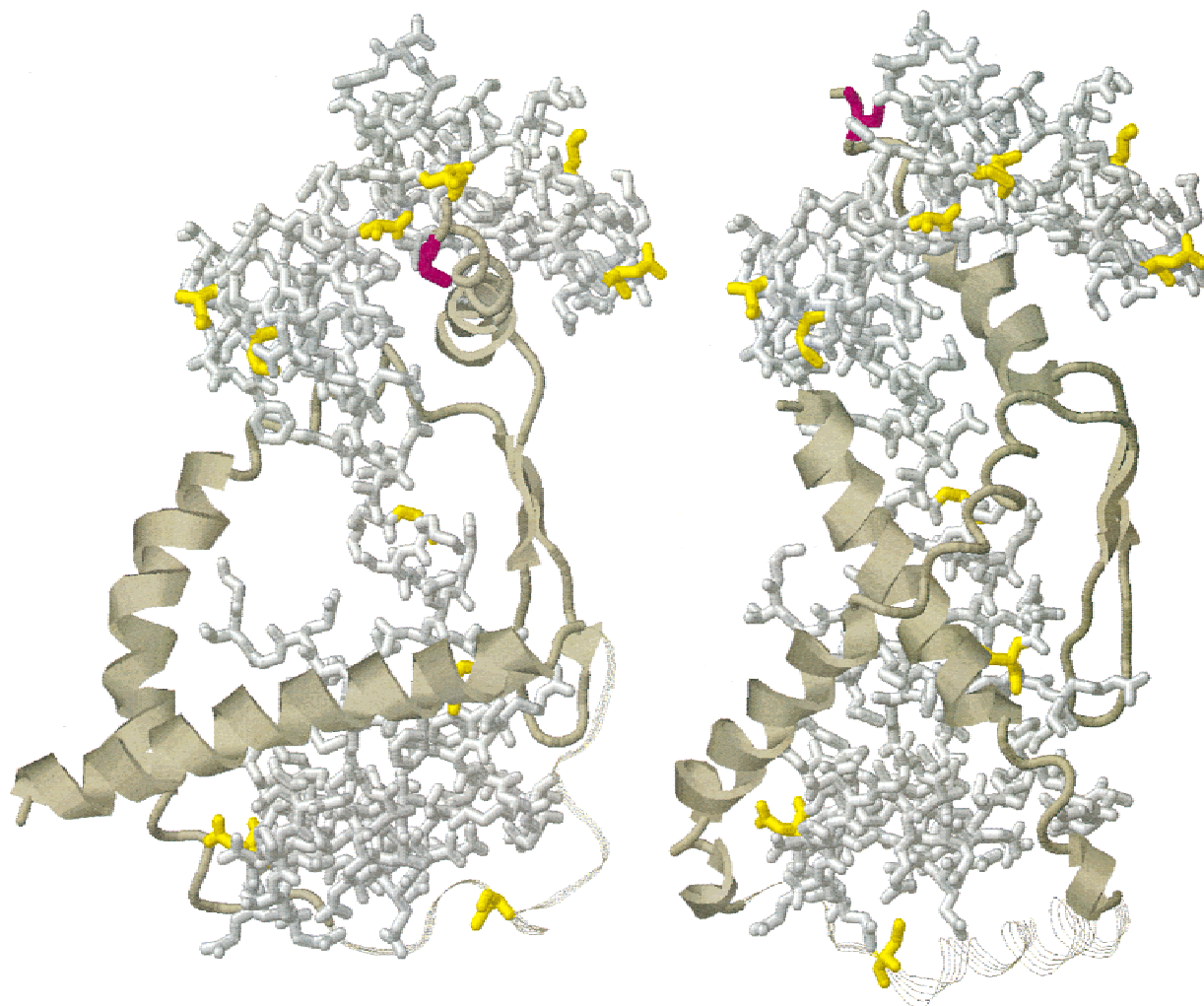


**Fig. 5.** Residues that have been labeled for FRET experiments. The donor label for all experiments was TnI133 (magenta). Acceptor labels (yellow) are listed in Table 2.

to the distance taken from both of our models. It may be significant that the experiment with the binary complex showed evidence for heterogeneity, while the experiment with the larger complex showed a single-exponential decay for the FRET signal.

### Discussion

We have presented two models of the interaction of TnI with TnC. The models are based on a low-resolution neutron scattering model of the overall folds of the components of the complex, and data from NMR and crystallography combined with computational modeling were used to develop an atomic-resolution view. An atomic-level model of TnC, modified to increase the opening of the N-terminal hydrophobic cleft, is a scaffold for five contiguous segments of TnI. A sixth unstructured TnI segment was not included. For the TnI models, there are varying amounts of experimental data available for each of the five segments. Segments I and V each have high-resolution experimental constraints derived from NMR or crystallographic structural models. In the case of segment V, there are also neutron scattering data supporting the models.

Segment IV, the inhibitory region, has been studied using NMR and is constrained by cross-linking to interact with both lobes of TnC. Segment III is constrained only by the neutron scattering data and requires further experimental data for refinement. Segment II, which is included only for the sake of completeness, is the most poorly constrained segment of the five segments modeled. Segment II and segment VI could potentially give rise to the diffuse features attributed to flexibility at the end-cap features of the original neutron scattering model (Olah & Trewhella, 1994).

The extended TnC structure in our models is based on shape and size information derived from neutron scattering studies (Olah et al., 1994; Olah & Trewhella, 1994; Stone et al., 1998). Comparisons with calmodulin/target enzyme interactions (reviewed in Trewhella, 1994; Ikura, 1996), and more recently the crystal structure of TnC/TnI(1–47) that shows a partially collapsed TnC (Vasyliev et al., 1998), have been used to argue that TnC adopts a collapsed conformation in its interaction with TnI. Both models suggest that the interactions required to maintain the extended conformation may only be present when TnC is in complex with intact TnI rather than a TnI fragment. It is also possible that crystal



packing forces induce the collapsed conformation of TnC in TnC/TnI(1–47). Calmodulin and TnC are structurally very similar, each consisting of two separate domains of EF-hand pairs linked by a flexible tether. There are data to indicate that the interconnecting helix regions of calmodulin and TnC play different roles, however, which may be anticipated in light of TnC having a single specialized function in muscle contraction in contrast to the many functions of calmodulin. Persechini et al. (1989) found that deletions in the central helix were not critical in target enzyme activation by calmodulin. By cross-linking calmodulin's globular lobes and cleaving the interconnecting helix region, they obtained a fully functional calmodulin (Persechini & Kretsinger, 1988). It was the report of this latter study that first described the “flexible tether” hypothesis for the function of calmodulin's central helix. In contrast, Ramakrishnan and Hitchcock-DeGregori (1995) concluded from TnC mutagenesis studies that the native length and structure of the central helix are optimal for normal regulatory function and that simple connectivity of the N- and C-terminal domains is insufficient for TnC function.

The flexible  $\beta$ -hairpin structure for TnI segment IV, corresponding to the inhibitory switch that binds alternately to actin and TnC in the contractile cycle, is the most important feature of our models. Even though models L and R were built independently, TnI segment IV is localized to the same region of TnC in both models. There are multiple experimental constraints from cross-linking and NMR that are consistent with this region of our model. The constraints do not allow determination of the precise conformation of the hairpin, but supporting evidence for our proposed structure for segment IV comes from the fact that a homologous region of profilin binds to actin in a similar long  $\beta$ -hairpin with a right-handed twist conformation. Flexibility in the hairpin would also be an important requirement for the switch function. Without the rest of the TnI sequence to serve as an anchor for the ends of the peptide, the loose  $\beta$ -hairpin structure would be expected to be unstable in solution, explaining the absence of observed interstrand nuclear Overhauser effects in our NMR study (Hernández et al., 1999).

We consider Models L and R to be equally likely descriptions of the interaction between TnI and TnC given the currently available experimental data. TnC has the same overall structure in both models, and both models have the same structure and localization of the inhibitory region, for which most of the cross-linking data are available. The secondary structure of TnI is the same in each model (except for unimportant differences in segment II), and the essential differences between the models are in the interaction of TnI segments I, III, and V with TnC (see Results). Segment III in Model R packs tightly against TnC without a gap such as is observed in Model L. The gap in Model L may facilitate binding to TnT. In Model R, the sandwiching of TnI segment I between TnI segment III and TnC topologically implies that TnI should bind to TnC first at the C-domain and then snake around TnC to interact with the N-domain. This ordering seems natural considering the function of the complex in the contractile cycle. Initially, when cellular  $\text{Ca}^{2+}$  levels are low, segment I of TnI binds to the C-domain of TnC, and segment V is free, allowing regions on either side of segment V to interact with actin. Then an increase in cellular  $\text{Ca}^{2+}$  causes segment V to bind to N-TnC, releasing the inhibitory interaction and allowing muscle to contract. Model L agrees better with the available crystallography and NMR data on the interactions of TnI segments I and V with TnC. In Model R, the 90° rotation of segment I causes TnI residues 14 and 19 to lose contact

with their neighbors on the C-domain of TnC, and the interaction of segment V with the N-domain of TnC differs from that in the NMR structure (Spyracopoulos et al., 2000). These experiments, however, were performed using peptide fragments of TnI, and, in the case of the NMR study, a single lobe of TnC. As we have described above, use of fragments can give rise to important changes, such as the degree of extension of the central helix of TnC or the conformation and binding site of the TnI inhibitory region. Future crystallography experiments may ultimately resolve the intact complex of TnI with TnC; however, the predicted flexibility of TnI in the binary complex may continue to inhibit its crystallization. At present more data from techniques such as small-angle scattering, cross-linking, and FRET using intact TnC/TnI will be useful in evaluating the relative success of the models, and to further refine each.

The most important difference between the model of TnI in the TnC/TnI interaction recently sketched by Luo et al. (2000) and our models is that Luo et al. propose an  $\alpha$ -helical structure for the inhibitory region, whereas we propose a  $\beta$ -hairpin structure for the inhibitory region. There is otherwise good apparent agreement in all segments in comparing the secondary structure of TnI. In comparing the interaction between TnI and TnC across studies, the model of Luo et al. most resembles our model L, with the placement of TnI segment I similar to that in the TnC/TnI(1–47) crystal structure, and the placement of segment V similar to that in the cardiac N-TnC/TnI(147–163) structure. The placement of segments II and III in the model of Luo et al. is significantly different from those in Model L. With respect to the interaction between TnI and TnC, there are no significant similarities between the model of Luo et al. and Model R.

While the original neutron scattering model of TnI in the complex (Olah & Trehwella, 1994) provided important clues about the overall fold of TnI, it was constructed by proposing geometrical shapes for each component of the model and varying the shape parameters to obtain maximum agreement with the data. As we did not have the capacity to model arbitrary, irregular shapes, the  $\beta$ -hairpin feature was not in the original model. The modifications to the models proposed here, based on addition of new data from many different experiments, preserves the essential feature of the original model—the central helical spiral. It is also likely that the diffuse “end-cap” features of the original model are caused by flexibility of segments II and VI in the binary complex.

Our discovery of the similarities between TnI and profilin suggest that the profilin/actin crystal structure (Schutt et al., 1995) could be used as a basis for designing new experiments to probe the TnI/actin interaction. For example, the alignment between profilin and TnI (Fig. 6) along with the profilin/actin crystal structure

	100	110	120	130
TNI	<u><b>NQKLFDLRGKFKR-PPLRRVRMSADAMLKALGSKHKV</b></u>			
	. . . . .	: . . . .	: . . . .	: . . . .
PROFILIN	<u><i>GEFTMDLRTKSTGGAPTFNITVTMTAKTLVLLMGKEGV</i></u>			
	90	100	110	

**Fig. 6.** Local sequence alignment of troponin-I with profilin. The alignment (boldface) is based on the longest sequence reported from a local alignment using the program LALIGN (Huang & Miller, 1991) of TnI residues 96–181 vs. the entire sequence of profilin. Also shown is a comparison of the five residues N-terminal to the aligned sequence (italics), which includes more residues in the inhibitory region of TnI (underlined). The symbol “.” indicates identity, and “:” indicates similarity.

(Fig. 7) suggests residues (e.g., TnI 105 and actin 288) that may be involved in the TnI/actin interaction. Hypotheses regarding specific interactions suggested by the model are amenable to mutagenesis testing by systematically replacing the above residues with alanine and looking for changes in binding (Gibbs & Zoller, 1991). Understanding the inhibitory switch of TnI may also lead to an increased understanding of the function of rabbit skeletal muscle phosphorylase kinase, whose sequence similarities with skeletal muscle TnI have been previously described (Dasgupta et al., 1989; Paudel & Carlson, 1990; Trehwella et al., 1990; Olah et al., 1994).

Our models of the TnC/TnI interaction suggest some interesting structural features of the  $\text{Ca}^{2+}$ -switch mechanism. In both models,

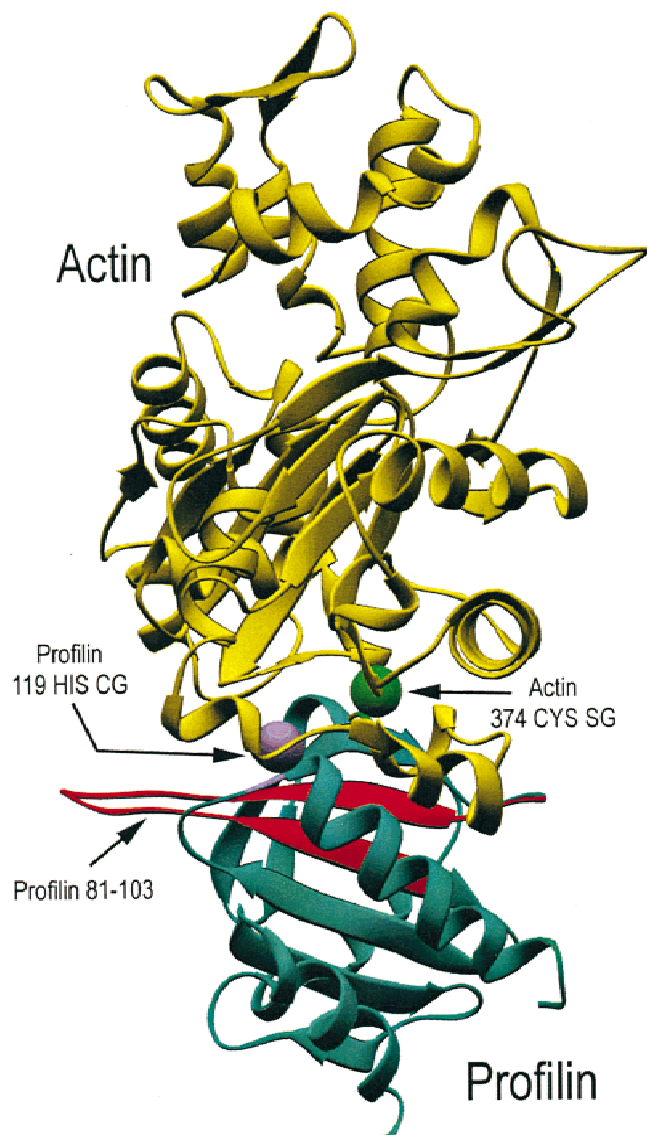


**Fig. 7.** Crystal structure of the profilin/actin complex. Profilin residues 81–103 (red), of which residues 86–103 align with the inhibitory region of TnI (see Fig. 6), lie at the interface between profilin (cyan) and actin (yellow) and form a  $\beta$ -hairpin with a right-handed twist, similar to the proposed model for TnI segment V. Profilin His119C $\gamma$  (lavender sphere) and actin Cys374S $\gamma$  (green sphere) are separated by 8.7 Å, which is favorable for cross-linking by BP-Mal. The alignment puts profilin His119 in register with TnI Cys133, which can form a BP-Mal cross-link to actin Cys374.

the two identified actin-binding domains—the TnI(96–115) inhibitory sequence (Syska et al., 1976), and TnI(140–148) (Tripet et al., 1997)—are on either side of the N-terminal hydrophobic cleft of TnC. This placement suggests a mechanism for simultaneous  $\text{Ca}^{2+}$ -induced modulation of the interactions of both actin-binding domains. NMR data (Slupsky & Sykes, 1995; McKay et al., 1998) indicate that binding of  $\text{Ca}^{2+}$  opens the N-terminal lobe of TnC, which favors a strong interaction between the hydrophobic cleft and TnI residues  $\sim$ 116–131. In binding to TnC, these TnI residues would pull both of the neighboring actin-binding domains (the inhibitory segment IV and residues 140–148 of segment VI) away from actin.  $\text{Ca}^{2+}$  dissociation from TnC would likewise release the TnI sequence segment  $\sim$ 116–131, leaving the actin-binding domains free to interact with actin and inhibit actomyosin ATPase. Similarities between TnI and profilin suggest that the  $\beta$ -hairpin structure of the inhibitory sequence segment IV may be well suited to flipping between binding sites on actin and TnC. The general features of this proposed mechanism for the TnC/TnI switch are the same as our previous proposal based on neutron scattering studies (Olah et al., 1994). There are also strong similarities to a model for the switch proposed by Tripet et al. (1997), except that in that model TnI(1–40) and the inhibitory region compete for binding to the C-terminal domain of TnC. This competitive binding is inconsistent with our model, as TnI(1–40) and the inhibitory region interact with different regions of TnC in our model.

Computational techniques are widely used to generate three-dimensional structural models. NMR and crystallography experiments yield hundreds to thousands of observables that are used in molecular dynamics refinements to produce models that are well constrained. When there are only scarce data available for an important system, as is often the case, computational approaches can be used to generate models that capture the essential topological features of interacting molecules, as we have demonstrated here. The troponin complex is too large for NMR studies of the intact proteins and has been stubbornly resistant to crystallization. A framework for modeling the interaction of TnI with TnC, however, was available in the shape information from the neutron scattering experiments. Our hybrid approach, using scattering data, crystallography and NMR data, model-building tools, and molecular dynamics methods for model building, and using cross-linking and FRET data for validation, has led to models of TnI topology that suggest novel, testable modes of TnC/TnI and TnI/actin interactions. As new data become available, the models will be further checked, adjusted, and refined, and as the accuracy increases it will further our understanding of the  $\text{Ca}^{2+}$ -switching mechanism in muscle contraction.

#### Materials and methods

Our models of TnC/TnI are based on a neutron scattering model obtained by neutron contrast variation experiments on the  $4\text{Ca}^{2+}$ /TnC/TnI complex with deuterated TnC (Olah et al., 1994; Olah & Trehwella, 1994). The neutron scattering experiments provided the vector length distribution function  $P(r)$  and radius of gyration  $R_g$  for both TnC and TnI in the binary complex. The values obtained for TnC are very similar to those calculated from the crystal structure of TnC (Herzberg & James, 1985). As the  $R_g$  value is extremely sensitive to the relative dispositions of the globular domains of TnC, the neutron scattering data provide good evidence that the interconnecting helix region of TnC in the binary complex is fully

extended. The neutron scattering data indicate that the separation of the globular domains is similar to that found in the crystal structure of isolated TnC. In an independent neutron scattering study, Stone et al. (1998) performed two neutron solvent matching experiments on a ternary TnC/TnI/TnT troponin complex in which either TnC or TnI was deuterated. These experiments yielded an  $R_g$  value for TnC that agrees with the extended structure found in the neutron scattering study of the binary complex. Both neutron scattering studies also found that TnI has a highly extended structure, although for TnI in the ternary complex the  $R_g$  value is 20% smaller than the value in the binary complex. This smaller  $R_g$  could be the result of TnI interactions with TnT that are missing in the binary complex.

#### *Modeling TnC in the complex*

The neutron scattering model of TnC in complex with TnI (Olah & Trehwella, 1994) was used as the scaffold about which to build TnI. This model has an "avian" sequence of TnC (Xu & Hitchcock-Degregori, 1988). The sequence consists of the residue segment 2–161 of chicken TnC (out of the 162 in Swiss-Prot accession P02588) with the following substitutions: Glu67Ala, Ala99Glu, and Asn100Asp. The avian TnC sequence is >99% identical to that of PDB accession number 5TNC, turkey skeletal muscle TnC, with the substitution Glu67Ala. For turkey TnC, substitutions Ala99Glu and Asn100Asp were identified crystallographically, as the sequence is not in public databases. No electron density is visible for the Glu67 side chain. Aside from the fact that chicken TnC has three extra residues (A, S, M) at the N-terminus, the rabbit and chicken sequences are 90.6% identical. All cross-linking and FRET experiments in the literature were performed using TnI and TnC from rabbit skeletal muscle. To facilitate comparisons with cross-linking and FRET data, therefore, all residue numbers for TnC in this paper correspond to the rabbit skeletal muscle sequence.

#### *Modeling TnI in the complex*

To model TnI, we began with sequence-based secondary structure predictions for rabbit skeletal muscle TnI and systematically applied experimental constraints to build each of the segments I–V. Only residues 3–134 in rabbit TnI were included in our model (this out of the 181 residues in Swiss-Prot accession P02643). Rabbit and chicken TnI are 83.1% identical, and the 3–134 segment of rabbit TnI is 78.8% identical to the equivalent segment in chicken TnI (LALIGN in Biology Workbench). The sequences (from Swiss-Prot Accession P02643) and secondary structure predictions for each segment are indicated in Figure 3. Over 78% of the protein is predicted to be  $\alpha$ -helical.

#### *Modeling TnI segment I*

In building Model R, the C-terminal domain of the crystal structure of TnC in complex with TnI(1–47) (Vassylyev et al., 1998, PDB accession number 1A2X) could not be directly grafted to our model without creating clashes with TnI segment III. Segment I was therefore docked onto the C-terminal domain of the neutron scattering model of TnC, after the model for segment III of TnI was built.  $C\alpha$  atom pairs between TnC and TnI that are separated by no more than 7 Å in the crystal structure were identified: TnC14–TnI7, TnC14–TnI11, TnC18–TnI4, TnC98–TnI22, TnC98–TnI25, TnC101–TnI25, TnC118–TnI21, TnC121–TnI24, TnC122–TnI24, TnC134–TnI14, TnC158–TnI19, and TnC159–TnI19. A

quadratic distance restraint with a force constant of 5 kcal mol<sup>-1</sup> Å<sup>-2</sup> was applied when the identified pairs of atoms were separated by more than 7 Å during the docking. Segment I was initially placed manually using the program MIDAS (Ferrin et al., 1988), and docking was then performed using a Monte Carlo approach. The initial segment I placement was randomly translated by up to 5 Å and rotated by up to 50° to generate an ensemble of 500 structures. Each of these structures was then equilibrated, using spring forces to enforce the distance restraints and a Van der Waals term to prevent clashes. The TnC model and TnI segment III were kept fixed during the equilibration. The lowest energy structure was selected for the model. In the final conformation in Model R, TnI segment I is rotated by nearly 90° with respect to the orientation in crystal structure and is approximately parallel with the central helix of TnC. Model L accommodates a placement of segment I with respect to TnC that closely resembles that in the crystal structure of Vassylyev et al. (1998).

#### *Modeling TnI segment II*

There are no structural data on this segment from crystallography or NMR experiments, and neutron scattering data (Olah & Trehwella, 1994) suggest that this part of TnI is unstructured in the binary complex. We included this segment, which is constrained to connect to segments I and III, to present a continuous model of TnI; the model illustrates an allowed rather than a preferred conformation of the backbone. For Model R, segment II was arbitrarily built with residues 34–45 as an  $\alpha$ -helical structure and residues 46–53 as a long loop, as is suggested by the secondary structure prediction. For Model L, the entire segment was arbitrarily built as a loop. Validation using the program PROCHECK (Lasowski et al., 1993) indicates that in both models the structure of this segment has acceptable geometry with no residues in forbidden regions of the Ramachandran plot. The structure of the loop was modeled using a previously described loop modeling procedure (Tung, 1997; Ryu et al., 1998) that efficiently generates stereochemically allowable loop conformations given fixed ends.

#### *Modeling TnI segment III*

In each model, the structure of this segment was defined by the spiral structure of TnI derived from neutron scattering experiments. A three-dimensional (3D) curve defining the center of the neutron scattering envelope was derived. To model the structure of segment III, we developed an algorithm to force an  $\alpha$ -helical polypeptide to follow the path of this 3D curve (see description below). A 41-amino acid  $\alpha$ -helical peptide was generated and then was rotated and translated along the curve. A position was chosen to place TnI segments III and V nearby, allowing for attachment to a  $\beta$ -hairpin structure for segment IV. Based on an analysis of known structures with  $\beta$ -hairpins (PDB accession codes 1F36, 1CMR, 1XBM), we chose a  $C\alpha$ – $C\alpha$  distance of 4.6 Å between the C-terminus of TnI segment III and the N-terminus of segment V.

#### *Modeling TnI segment IV, the inhibitory region*

Recent CD and NMR studies of 1:1 complexes of 4Ca<sup>2+</sup>/TnC and TnI(96–115) (Hernández et al., 1999) show that TnC-bound TnI(96–115) assumes an extended conformation. The NMR data in that study indicate that there is a kink at Gly104. Cross-linking (Leszyk et al., 1987; Kobayashi et al., 1994, 1996; Ngai et al., 1994; Jha et al., 1996) and fluorescence data (Tao et al., 1989; Pearlstone & Smillie, 1995; Luo et al., 1997, 1998; Pearlstone et al., 1997) indicate that TnI(96–115) interacts with both the N-



and C-terminal domains of TnC. We therefore decided to propose a  $\beta$ -hairpin structure for segment IV. This structure can reach from the N- to the C-terminal domain of TnC, satisfies the requirements for the segment to have an extended structure, and can be made to have a kink at Gly104 by placing that residue within the turn region of the hairpin. In each model, the hairpin was built with a right-handed twist by the same loop-building program as was used to construct segment II. Two additional loops were built to connect the hairpin to both the C-terminus of segment III and the N-terminus of segment V.

#### Modeling TnI segment V

NMR data (McKay et al., 1997, 1998, 1999) indicate that residues ~115–131 interact with the N-terminal domain of TnC, with close interactions in the hydrophobic cleft of this region of TnC. Our previous TnC/TnI model (Olah & Trewthella, 1994) based on the neutron scattering data (Fig. 2) shows a superhelical curve going through the N-terminal hydrophobic cleft. Both secondary structure prediction and the dimensions of the neutron scattering model indicate that segment V adopts a mostly  $\alpha$ -helical conformation. For both Model L and Model R, the segment was built in a similar fashion to the construction of the segment III model (described above), following the curve of the neutron scattering model. A Van der Waals term was included in the rotation and translation search to avoid clashes with the N-terminal domain of TnC.

#### Modeling curved $\alpha$ -helical structures

Based on secondary structure analysis and the models derived from neutron scattering data, a large part of TnI (segment III and V) adopts an  $\alpha$ -helical structure that spirals around TnC. Using a method similar to that developed to generate DNA double helical structures along prescribed curves in three dimensions (Tung & Soumpasis, 1995), we developed an algorithm to generate an  $\alpha$ -helix that follows a specified 3D curve. The resulting curved  $\alpha$ -helix is visualized to confirm the secondary structure, and the program PROCHECK (Lasowski et al., 1993) is used to validate the stereochemistry. This algorithm was used to generate a supercoiled helix that fits the central spiral shape in the neutron scattering model for TnI. The spiral is represented as a uniform distribution of random points within the envelope of the neutron model. A group of points along the center of the spiral is selected to serve as guiding points for generating a smooth curve using a standard B-spline interpolating algorithm (Hao & Olson, 1989). The curve is then sampled by points positioned at 1.48 Å intervals along the curve (1.48 Å is the projection onto the helix axis of the distance vector between neighboring C $\alpha$  atoms in a  $\alpha$ -helix). Residues are placed around the curve in a typical  $\alpha$ -helical pattern, with all of the C $\alpha$  atoms at a distance 2.40 Å from the curve, and at a pitch of 3.75 residues per turn. The precise placement of the first residue defines the orientation and translation of the helix within the constraints of the curve. In applying this method to models of TnI, segment V was built before segment III. The segment V  $\alpha$ -helix was rotated and translated to minimize the value of a target function that consisted of a Van der Waals energy plus a restraint derived from cross-linking data. The cross-linking restraint was later relaxed for model refinement. After segment V was built, segment III was fit to the curve of the superhelical neutron scattering envelope and was translated and rotated to accommodate a  $\beta$ -hairpin structure for segment IV.

#### Model refinement

The program AMBER (Weiner et al., 1986) was used for energy minimizations. The stereochemistry of the energy-minimized model was evaluated using the program PROCHECK (Lasowski et al., 1993), which reported 72 and 76% of residues in the “most favored regions” area of the Ramachandran plot for Models R and L, respectively. Several bond lengths, angles, planar groups, and Van der Waals contacts were also flagged for improvement. To improve the stereochemistry, models were refined by a recently developed molecular dynamics method that makes use of interatomic distance probabilities derived from known protein structures (see Subramaniam et al., 1996 for a detailed description of the distance probabilities, and Wall et al., 1999 for a detailed description of the molecular dynamics method). A likelihood for an atomic-level model is constructed from the product of interatomic distance probabilities, using an assumption that each atom pair contributes independently. By analogy with Boltzmann statistics, an energy function is then derived that is proportional to the negative log of the likelihood. A molecular dynamics simulation at 300 K was performed using a version of the program X-PLOR (Brünger, 1993) modified to use this energy function. The standard Van der Waals potential was replaced by the PDF potential, and geometrical restraints on bonds, bond angles and dihedral angles were used. A weak electrostatic interaction was used to provide attraction between TnC and TnI (no electrostatic interaction was included between any two atoms on the same molecule). For the electrostatic interaction, all atoms on TnC were assigned a positive charge of one electron, and all atoms on TnI were assigned a negative charge of 0.01 electrons. A harmonic potential (“harmonic = 50.0” and “exponent=2” in X-PLOR) was used to restrain the atomic positions in the N-domain of TnC, and a similar potential (“harmonic = 5.0” and “exponent=2”) was used to weakly restrain the atomic positions in the  $\beta$ -hairpin. A total of 100 models were output once every 50 cycles of simulated annealing. To improve geometry, the best structure as evaluated using PROCHECK (Lasowski et al., 1993) was then subjected to 500 cycles of simulated annealing at 100 K using a Van der Waals potential and geometrical restraints. A harmonic potential (“harmonic = 50.0” and “exponent=2”) was used to restrain the positions of all atoms in the model. The structure was finally subjected to Powell minimization for 500 cycles using similar energy terms, but with a weaker harmonic restraint (“harmonic = 10.0”). Both final Models R and L had acceptable stereochemistry, as reported in Results.

#### Model validation using cross-linking data

For model validation, we only used cross-linking data that gave sufficiently detailed contact information between polypeptide chains. To qualify as a validation criterion, an identified cross-link had to be localized to a segment smaller than 20 residues on both chains, and to a single residue on at least one of the chains. Cross-linking data for TnC21 (Leszyk et al., 1988) are included in Table 1 because mass spectrometry was used to identify cross-links at multiple sites throughout TnI(96–134). Three methods of cross-linking were used in the studies we found in our literature search: cross-linking using 4-maleimidobenzophenone (BP-Mal) as a linker; cross-linking using benzophenone-4-iodoacetamide (BP-IA) as a linker; and 1-ethyl-3-[3-(dimethylamino)propyl]carbodiimide (EDC) zero-length cross-linking. BP-Mal cross-links form by covalent attachment of the maleimide moiety to a cysteine S $\gamma$  and



subsequent photo-activated attachment of the benzophenone function to a C-H carbon. BP-IA cross-links are similar but with covalent attachment of the iodoacetamide moiety to a cysteine S $\gamma$ . Any nonaromatic C-H is a possible target for photo-cross-linking, so long as there is no steric hindrance and the electronic orbitals are favorable. The most favorable cross-linking targets, however, are Val C $\beta$ , Leu C $\gamma$ , Met C $\gamma$ , Arg C $\delta$ , and Lys C $\epsilon$  (based on comments in Dorman & Prestwich, 1994). EDC zero-length cross-links are between a side chain amide nitrogen and a side-chain carboxyl oxygen.

To determine whether the existing cross-linking data are consistent with a model, for each reported cross-link, distances were measured between the known reactive atom on TnC (the cross-link was always localized to a single residue on TnC) and reactive atoms in likely target residues on TnI. To make use of data from experiments that used mutant proteins, a corresponding atom was chosen that mimicked the position of the chemically active atom in the mutant residue. The smallest distance found in each of the experiments is reported in Table 2. The expected distance between reactive groups linked by BP-Mal is <9 Å, the length of the BP-Mal molecule (Tao et al., 1990). The expected distance between reactive groups linked by BP-IA is <10 Å, based on our estimate derived from a comparison with BP-Mal. For EDC cross-linking, the cross-linked reactive groups form an amide bond, which is shorter than the closest distance between the corresponding atoms in the protein. Therefore these distances are 3 Å, close to the Van der Waals contact distance. Our criterion for determining whether a distance would accommodate a cross-link is that the measured distance is no more than 2.5 Å greater than the expected distance, accounting for dynamics in the structure. Even if a conformation that brings two residues close enough to cross-link is relatively unfavorable thermodynamically, the irreversibility of the process means that, so long as it occurs with some small frequency, the cross-link will be observed experimentally.

#### Sequence alignment of TnI and profilin

The sequence of TnI was aligned with bovine profilin using the program LALIGN (Huang & Miller, 1991) in the Biology Workbench Version 3.0. LALIGN is a program in the fasta20u63 distribution by W.R. Pearson, University of Virginia, and the Biology Workbench was developed by Subramaniam et al. (1996) at the National Center for Supercomputing Applications at the University of Illinois at Urbana-Champaign, access by the internet at biology.ncsa.uiuc.edu. Input sequences were the residue 96–181 segment of rabbit TnI (Swiss-Prot accession P02643) that begins at the inhibitory region and contains the actin-binding regions, and the sequence of bovine profilin from PDB entry 2BTF. The default scoring matrix (BLOSUM50) and gap penalties (–12/–2) were used. The alignment matched TnI residues 101–133 with profilin residues 86–118. This sequence alignment was the longest reported, with 30.3% identity and a gap inserted after TnI 109 (Fig. 6).

#### Note added in proofs

After the acceptance of this manuscript, Zhao et al. (2000) published FRET distances between wild-type rabbit skeletal muscle TnC and a TnI mutant with no Cys residues and a Trp at position 106. In the presence of Ca<sup>2+</sup>, the average distance between TnI Trp106 and labels at TnC Met25 and TnC Cys98 was measured to

be 22 Å and 20 Å, respectively. In model L the distances between corresponding C $\alpha$  pairs are 47 Å and 16 Å, and in model R the distances are 46 Å and 12 Å.

#### Acknowledgments

We gratefully acknowledge Donald K. Blumenthal for critically reading the manuscript and an anonymous reviewer for excellent suggestions. This work was performed under the auspices of the Department of Energy under contract to the University of California and was supported by DOE BER project KP1101010 (J.T.), NIH grant GM40528 (J.T.), and the Integrated Structural Biology Resource supported by Laboratory Directed Research and Development at Los Alamos National Laboratory (C.T.).

#### References

- Berman HM, Westbrook J, Feng Z, Gilliland G, Bhatt TN, Weissig H, Shindyalov IN, Bourne PE. 2000. The Protein Data Bank. *Nucleic Acids Res* 28:235–242.
- Blechner SL, Olah GA, Strynadka NCJ, Hodges RS, Trewhella J. 1992. 4Ca<sup>2+</sup>-troponin-C forms dimers in solution at neutral pH that dissociate upon binding various peptides: Small-angle X-ray-scattering studies of peptide-induced structural changes. *Biochemistry* 31:11326–11334.
- Brünger AT. 1993. *X-PLOR version 3.1: A system for X-ray crystallography and NMR*. New Haven, CT: Yale University Press.
- Campbell PA, Sykes BD. 1991. Interaction of troponin I and troponin C. Use of the two-dimensional nuclear magnetic resonance transferred nuclear Overhauser effect to determine the structure of the inhibitory troponin I peptide when bound to skeletal troponin C. *J Mol Biol* 222:405–421.
- Carlsson L, Nyström LE, Sunkvist I, Markey F, Lindberg U. 1977. Actin polymerizability is influenced by profilin, a low molecular weight protein in non-muscle cells. *J Mol Biol* 115:465–483.
- Chandra M, McCubbin WD, Oikawa K, Kay CM, Smillie LB. 1994. Ca<sup>2+</sup>, Mg<sup>2+</sup>, and troponin I inhibitory peptide binding to a Phe-154 to Trp mutant of chicken skeletal muscle troponin C. *Biochemistry* 33:2961–2969.
- Dasgupta M, Honeycutt T, Blumenthal D. 1989. The  $\gamma$ -subunit of skeletal muscle phosphorylase kinase contains two noncontiguous domains that act in concert to bind calmodulin. *J Biol Chem* 264:17156–17163.
- Deleage G, Roux B. 1987. An algorithm for protein secondary structure prediction based on class prediction. *Prot Eng* 1:289–294.
- Dorman G, Prestwich GD. 1994. Benzophenone photophores in biochemistry. *Biochemistry* 33:5661–5673.
- Farah CS, Miyamoto CA, Ramos CH, da Silva AC, Quaggio RB, Fujimori K, Smillie LB, Reinach. 1994. Structural and regulatory functions of the NH<sub>2</sub>- and COOH-terminal regions of skeletal muscle troponin I. *J Biol Chem* 269:5230–5240.
- Farah CS, Reinach FC. 1995. The troponin complex and regulation of muscle contraction. *FASEB J* 9:755–767.
- Ferrin TE, Huang CC, Jarvis LE, Langridge R. 1988. The MIDAS display system. *J Mol Graphics* 6:13–27.
- Gagné SM, Tsuda S, Li M, Smillie LB, Sykes BD. 1995. Structures of the troponin C regulatory domains in the apo and calcium-saturated states. *Nat Struct Biol* 2:784–789.
- Georjun C, Deleage G. 1994. SOPMA: A self-optimized method for protein secondary structure prediction. *Protein Eng* 7:157–164.
- Georjun C, Deleage G. 1995. SOPMA: Significant improvements in protein secondary structure prediction by consensus prediction from multiple alignments. *CABIOS* 11:681–684.
- Gibbs CS, Zoller MJ. 1991. Rational scanning mutagenesis of a protein-kinase identifies functional regions involved in catalysis and substrate interactions. *J Biol Chem* 266:8923–8931.
- Hao M-H, Olson WK. 1989. Modeling DNA supercoils and knots with B-spline functions. *Biopolymers* 28:873–900.
- Heidorn DB, Trewhella J. 1988. Comparison of the crystal structures of calmodulin and troponin C. *Biochemistry* 27:909–915.
- Hernández G, Blumenthal DK, Kennedy MA, Unkefer CJ, Trewhella J. 1999. Troponin I inhibitory peptide (96–115) has an extended conformation when bound to skeletal muscle troponin C. *Biochemistry* 38:6911–6917.
- Herzberg O, James MNG. 1985. Structure of the calcium regulatory muscle protein troponin-C at 2.8 Å resolution. *Nature* 313:653–659.
- Herzberg O, James MNG. 1988. Refined crystal structure of troponin C from turkey skeletal muscle at 2.0 Å resolution. *J Mol Biol* 203:761–779.

- Herzberg O, Moulton J, James MNG. 1986. A model for the  $\text{Ca}^{2+}$ -induced conformational transition of troponin C. A trigger for muscle contractions. *J Biol Chem* 261:2638–2644.
- Houdusse A, Love ML, Dominguez R, Grabarek Z, Cohen C. 1997. Structures of  $4\text{Ca}^{2+}$ -bound troponin C at 2.0 Å resolution: Further insights into the  $\text{Ca}^{2+}$ -switch in the calmodulin superfamily. *Structure* 5:1695–1711.
- Huang X, Miller W. 1991. A time-efficient, linear-space local similarity algorithm. *Adv Appl Math* 12:337–357.
- Ikura M. 1996. Calcium binding and conformational response in EF-hand proteins. *TIBS* 21:14–17.
- Jha PK, Mao C, Sarkar S. 1996. Photo-cross-linking of rabbit skeletal troponin I deletion mutants with troponin C and its thiol mutants: The inhibitory region enhances binding of troponin I fragments to troponin C. *Biochemistry* 35:11026–11035.
- Kobayashi T, Leavis PC, Collins JH. 1996. Interaction of a troponin I inhibitory peptide with both domains of troponin C. *Biochim Biophys Acta* 1294:25–30.
- Kobayashi T, Tao T, Gergely J, Collins JH. 1994. Structure of the troponin complex: Implications of photocross-linking of troponin I to troponin C thiol mutants. *J Biol Chem* 269:5725–5729.
- Kobayashi T, Tao T, Grabarek Z, Gergely J, Collins JH. 1991. Cross-linking of residue 57 in the regulatory domain of a mutant rabbit skeletal muscle troponin C to the inhibitory region of troponin I. *J Biol Chem* 266:13746–13751.
- Kobayashi T, Zhao X, Wade R, Collins J. 1999.  $\text{Ca}^{2+}$ -dependent interaction of the inhibitory region of troponin I with acidic residues in the N-terminal domain of troponin C. *Biochim Biophys Acta* 1430:214–221.
- Kretsinger RH. 1976. Calcium-binding proteins. *Ann Rev Biochem* 45:239–266.
- Krudy GA, Kleerekoper Q, Guo X, Howarth JW, Solaro RJ, Rosevear PR. 1994. NMR studies delineating spatial relationships within the cardiac troponin I-troponin C complex. *J Biol Chem* 269:23731–23735.
- Lasowski RA, MacArthur MW, Moss DS, Thornton JM. 1993. PROCHECK: A program to check the stereochemical quality of protein structures. *J Appl Crystallogr* 26:283–291.
- Leszyk J, Collins JH, Leavis PC, Tao T. 1987. Cross-linking of rabbit skeletal muscle troponin with the photoreactive reagent 4-maleimidobenzophenone: Identification of residues in troponin I that are close to cysteine-98 of troponin C. *Biochemistry* 26:7042–7047.
- Leszyk J, Collins JH, Leavis PC, Tao T. 1988. Cross-linking of rabbit skeletal muscle troponin subunits: Labeling of cysteine-98 of troponin C with 4-maleimidobenzophenone and analysis of products formed in the binary complex with troponin T and the ternary complex with troponins I and T. *Biochemistry* 27:6983–6987.
- Leszyk J, Grabarek Z, Gergely J, Collins JH. 1990. Characterization of zero-length cross-links between rabbit skeletal muscle troponin C and troponin I: Evidence for direct interactions between the inhibitory region and the  $\text{NH}_2$ -terminal, regulatory domain of troponin C. *Biochemistry* 29:299–304.
- Leszyk J, Tao T, Nuwaysir LM, Gergely J. 1998. Identification of the photocrosslinking sites in troponin-I with 4-maleimidobenzophenone labelled mutant troponin-Cs having single cysteines at positions 158 and 21. *J Muscle Res Cell Motil* 19:479–490.
- Levin JM, Robson B, Garnier J. 1986. An algorithm for secondary structure determination in proteins based on sequence similarity. *FEBS Lett* 205:303–308.
- Li MX, Spyropoulos L, Sykes BD. 1999. Binding of cardiac troponin-I<sub>147-163</sub> induces a structural opening in human cardiac troponin-C. *Biochemistry* 38:8289–8298.
- Luo Y, Leszyk J, Qian Y, Gergely J, Tao T. 1999. Residues 48 and 82 at the N-terminal hydrophobic pocket of rabbit skeletal muscle troponin-C photocross-link to Met121 of troponin-I. *Biochemistry* 38:6678–6688.
- Luo Y, Wu J-L, Gergely J, Tao T. 1997. Troponin T and  $\text{Ca}^{2+}$  dependence of the distance between Cys48 and Cys133 of troponin I in the ternary troponin complex and reconstituted thin filaments. *Biochemistry* 36:11027–11035.
- Luo Y, Wu J-L, Gergely J, Tao T. 1998. Localization of Cys133 of rabbit skeletal troponin-I with respect to troponin-C by resonance energy transfer. *Biophys J* 74:3111–3119.
- Luo Y, Wu J-L, Li B, Langsetmo K, Gergely J, Tao T. 2000. Photocrosslinking of benzophenone-labeled single cysteine troponin I mutants to other thin filament proteins. *J Mol Biol* 296:899–910.
- McKay RT, Pearlstone JR, Corson DC, Gagne SM, Smillie LB, Sykes BD. 1998. Structure and interaction site of the regulatory domain of troponin-C when complexed with the 96–148 region of troponin-I. *Biochemistry* 37:12419–12430.
- McKay RT, Triplet BP, Hodges RS, Sykes BD. 1997. Interaction of the second binding region of troponin I with the regulatory domain of skeletal muscle troponin C as determined by NMR spectroscopy. *J Biol Chem* 272:28494.
- McKay RT, Triplet BP, Pearlstone JR, Smillie LB, Sykes BD. 1999. Defining the region of troponin-I that binds to troponin-C. *Biochemistry* 38:5478–5489.
- Ngai S-M, Sönnichsen FD, Hodges RS. 1994. Photochemical cross-linking between native rabbit skeletal troponin C and benzoylbenzoyl-troponin I inhibitory peptide, residues 10-115. *J Biol Chem* 269:2165–2172.
- Nodelman IM, Bowman GD, Lindberg U, Schutt CE. 1999. X-ray structure determination of human profilin II: A comparative structural analysis of human profilins. *J Mol Biol* 294:1271–1285.
- Olah GA, Rokop SE, Wang C-LA, Blechner SL, Trehwella J. 1994. Troponin I encompasses an extended troponin C in the  $\text{Ca}^{2+}$  bound complex: A small-angle X-ray and neutron scattering study. *Biochemistry* 33:8233–8239.
- Olah GA, Trehwella J. 1994. A model structure of the muscle protein complex  $4\text{Ca}^{2+}$ /troponin C/troponin I derived from small-angle scattering data: Implications for regulation. *Biochemistry* 33:12800–12806.
- Paudel HK, Carlson GM. 1990. Functional and structural similarities between the inhibitory region of troponin I coded by exon VII and the calmodulin-binding regulatory region of the catalytic subunit of phosphorylase kinase. *PNAS* 87:7285–7289.
- Pearlstone JR, Smillie LB. 1985. The interaction of rabbit skeletal muscle troponin-T fragments with troponin-I. *Can J Biochem Cell Biol* 63:212–218.
- Pearlstone JR, Smillie LB. 1995. Evidence for 2-site binding of troponin-I inhibitory peptides to the N-domain and C-domain of troponin-C. *Biochemistry* 34:6932–6940.
- Pearlstone JR, Sykes BD, Smillie LB. 1997. Interactions of structure C and regulatory N domains of troponin C with repeated sequence motifs in troponin I. *Biochemistry* 36:7601–7606.
- Perry SV. 1999. Troponin I: Inhibitor or facilitator. *Mol Cell Biochem* 190:9–32.
- Persechini A, Blumenthal DK, Jarrett HW, Klee CB, Hardy DO, Kretsinger RH. 1989. The effects of deletions in the central helix of calmodulin on enzyme activation and peptide binding. *J Biol Chem* 264:8052–8058.
- Persechini A, Kretsinger RH. 1988. The central helix of calmodulin functions as a flexible tether. *J Biol Chem* 263:12175–12173.
- Potter JD, Gergely J. 1975. The calcium and magnesium binding sites on troponin and their role in the regulation of myofibrillar adenosine triphosphatase. *J Biol Chem* 250:4628–4633.
- Ramakrishnan S, Hitchcock-DeGregori SE. 1995. Investigation of the structural requirements of the troponin C central helix for function. *Biochemistry* 34:16789–16796.
- Rost B, Sander C. 1994. Combining evolutionary information and neural networks to predict protein secondary structure. *Proteins Struct Funct Genet* 19:55–72.
- Ryu KS, Lee HY, Kim SP, Beauchamp J, Tung C-S, Issacs NW, Ji IH, Ji TH. 1998. Modulation of high affinity hormone binding: Human choriogonadotropin binding to the exodomain of the receptor is influenced by exoloop-2 of the receptor. *J Biol Chem* 273:6285–6291.
- Satyshur KA, Rao ST, Pyzalska D, Drendel W, Greaser M, Sundaralingam M. 1988. Refined structure of chicken skeletal muscle troponin C in the two-calcium state at 2 Å resolution. *J Biol Chem* 263:1628–1647.
- Schutt CE, Myslik JC, Rozycki MD, Goonesekere NCW, Lindberg U. 1995. The structure of crystalline profilin-β-actin. *Nature* 365:810–816.
- Slupsky CM, Sykes BD. 1995. NMR solution structure of calcium-saturated skeletal muscle troponin C. *Biochemistry* 34:1628–1647.
- Soman J, Tao T, Phillips GN Jr. 1999. Conformational variation of calcium-saturated rabbit skeletal troponin C. *Proteins* 37:510–511.
- Spyropoulos L, McKay RT, Sykes BD. 2000. Structure of skeletal troponin-C in complex with skeletal troponin-I<sub>115-131</sub>: Comparison to cardiac troponin-C-troponin-I<sub>147-163</sub> complex. *Biophys J* 78:434A.
- Stefancsik R, Jha PK, Sarkar S. 1998. Identification and mutagenesis of a highly conserved somain in troponin T responsible for troponin I binding—Potential role for coiled coil interaction. *Proc Natl Acad Sci USA* 95:957–962.
- Stone DB, Timmins PA, Schneider DK, Krylova I, Ramos CHI, Reinach FC, Mendelson RA. 1998. The effect of regulatory  $\text{Ca}^{2+}$  on the in situ structures of troponin C and troponin I: A neutron scattering study. *J Mol Biol* 281:689–704.
- Strynadka NCJ, Cherney M, Sielecki AR, Li MX, Smillie LB, James MNG. 1997. Structural details of a calcium-induced molecular switch: X-ray crystallographic analysis of the calcium-saturated N-terminal domain of troponin C at 1.75 Å resolution. *J Mol Biol* 273:238–255.
- Subramaniam S, Tchong DK, Fenton JM. 1996. In: States DJ, Agarwal P, Gasterland T, Hunter L, Smith RF, eds. *Proceedings of the fourth international conference on intelligent systems in molecular biology*, St. Louis. Menlo Park, CA: AAAI Press. pp 218–229.
- Syska H, Wilkinson JM, Grand JA, Perry SV. 1976. Relationship between biological-activity and primary structure of troponin-I from white skeletal-muscle of rabbit. *Biochem J* 153:375–387.
- Szczesna D, Zhang R, Zhao J, Jones M, Potter JD. 1999. The role of the  $\text{NH}_2$ - and  $\text{COOH}$ -terminal domains of the inhibitory region of troponin I in the regulation of skeletal muscle contraction. *J Biol Chem* 274:29536–29542.
- Tao T, Gong BJ, Leavis PC. 1990. Calcium-induced movement of troponin-I relative to actin in skeletal muscle thin filaments. *Science* 247:1339–1341.

- Tao T, Gowell E, Strasburg GM, Gergely J, Leavis PC. 1989.  $\text{Ca}^{2+}$  dependence of the distance between Cys-98 of troponin C and Cys-133 of troponin I in the ternary complex. Resonance energy transfer measurements. *Biochemistry* 28:5902–5908.
- Tobacman LS. 1996. Thin filament mediated regulation of cardiac contraction. *Ann Rev Physiol* 58:447–481.
- Trewhella J. 1994. Conformational flexibility in biochemical regulation. In: Ramaswamy HS, Mukti HS, eds. *Structural biology: State of the art*. New York: Adenine Press. pp 43–57.
- Trewhella J, Blumenthal DK, Rokop SE, Seeger PA. 1990. Small-angle scattering studies show distinct conformations of calmodulin in its complexes with two peptides based on the regulatory domain of the catalytic sub unit of phosphorylase kinase. *Biochemistry* 29:9316–9324.
- Tripet B, Van Eyk JE, Hodges RS. 1997. Mapping of a second actin-tropomyosin and a second troponin C binding site within the C terminus of troponin I, and their importance in the  $\text{Ca}^{2+}$ -dependent regulation of muscle contraction. *J Mol Biol* 271:728–750.
- Tung C-S. 1997. A computational approach to modeling nucleic acid hairpin structures. *Biophys J* 72:876–885.
- Tung C-S, Soumpasis DM. 1995. The construction DNAa helical duplexes along prescribed 3D curves. *J Biomol Struct Dyn* 13:577–582.
- Van Eyk JE, Strauss JD, Hodges RS, Ruegg JC. 1993. A synthetic peptide mimics troponin I function in the calcium-dependent regulation of muscle contraction. *FEBS Lett* 323:223–228.
- Vassilyev DG, Takeda S, Wakatsuki S, Maeda K, Maeda Y. 1998. Crystal structure of troponin C in complex with troponin I fragment at 2.3-Å resolution. *Proc Natl Acad Sci* 95:4847–4852.
- Wall ME, Subramaniam S, Phillips GN Jr. 1999. Protein structure determination using a database of interatomic distance probabilities. *Protein Sci* 8:2720–2727.
- Wang C-K, Cheung HC. 1984. Proximity relationship in the binary complex formed between troponin I and troponin C. *J Mol Biol* 190:509–521.
- Weiner SJ, Kollman PA, Nguyen DT, Case DA. 1986. An all atom force field for simulations of proteins and nucleic acids. *J Comp Chem* 7:230–252.
- Wilkinson JM, Grand RJA. 1978. Comparison of amino acid sequences of troponin I from different striated muscle. *Nature* 271:31.
- Xu G-Q, Hitchcock-Degregori SE. 1988. Synthesis of a troponin C cDNA and expression of wild type and mutant proteins in *Escherichia coli*. *J Biol Chem* 263:13962–13969.
- Zhao X, Kobayashi T, Gryczynski Z, Gryczynski I, Lakowicz J, Wade R, Collins JH. 2000. Calcium-induced flexibility changes in the troponin C–troponin I complex. *Biochim Biophys Acta* 1479:247–254.